APPLIED AND ENVIRONMENTAL MICROBIOLOGY, Apr. 1992, p. 1175–1182
0099-2240/92/041175-08$02.00/0

Vol. 58, No. 4

Corrosion and Electrochemical Oxidation of a Pyrite by *Thiobacillus ferrooxidans*

C. MUSTIN,[1]* J. BERTHELIN,[1] P. MARION,[2] AND P. DE DONATO[2]

Centre de Pédologie Biologique du C.N.R.S., UPR 6831 Associée à l'Université de Nancy I, 17 Rue Notre-Dame-des-Pauvres, B.P. 5,[1] and Ecole Nationale Supérieure de Géologie, Laboratoire "Environnement et Minéralurgie," U.R.A. 235 du C.N.R.S., B.P. 40,[2] 54501 Vandœuvre-les-Nancy Cedex, France

Received 23 July 1991/Accepted 31 January 1992

The oxidation of a pure pyrite by *Thiobacillus ferrooxidans* is not really a constant phenomenon; it must be considered to be more like a succession of different steps which need characterization. Electrochemical studies using a combination of a platinum electrode and a specific pyrite electrode (packed-ground-pyrite electrode) revealed four steps in the bioleaching process. Each step can be identified by the electrochemical behavior (redox potentials) of pyrite, which in turn can be related to chemical (leachate content), bacterial (growth), and physical (corrosion patterns) parameters of the leaching process. A comparison of the oxidation rates of iron and sulfur indicated the nonstoichiometric bacterial oxidation of a pure pyrite in which superficial phenomena, aqueous oxidation, and deep crystal dissolution are successively involved.

Since its discovery (5, 6), the acidophilic iron-oxidizing bacterium *Thiobacillus ferrooxidans* has been used for the recovery of copper and uranium from low-grade ores in industrial heap, dump, and in situ leaching processes (26) and more recently in a pilot plant for gold extraction (11, 13). Knowledge of the physiology, biochemistry, and genetic characteristics of the bacteria and of the leaching processes is growing (3, 10, 11). Despite this interest and the important results presented in many articles, the mechanisms and processes involved in bioleaching are poorly understood. To increase knowledge on the subject, different fundamental studies of acidophilic iron- and sulfur-oxidizing bacteria, the nature of the bacterium-mineral (sulfide) interface, and the reactions occurring at the interface are required. Pyrite oxidation in the presence of *T. ferrooxidans* involves not only direct action by the bacterium but also chemical oxidation by ferric ions produced by the bacteria and released in the leachate (16, 23).

The strictly chemical oxidation and electrochemical dissolution of pyrite have been discussed (18–20), but only a few works have been done on observing a relationship between electrochemical properties and physical-chemical evolution during the bacterial leaching process (15). Measurements of the redox potential of a ground-pyrite suspension during oxidation by *T. ferrooxidans* have been determined and provided information only on a global redox condition of the pulp (2). The redox potential of pyrite was used to measure the chemical activity of bacteria and the oxidation rate of iron (17, 22) but only during very short incubation periods that do not correspond to complete leaching or weathering processes.

Moreover, the measurement of pyrite redox potential in those experiments was performed with a pyrite slab electrode that does not represent the diversity of pyrite grains and which consequently promoted the influence of only one major crystalline orientation. Crystalline orientation can strongly modify the resistivity and semiconductivity of pyrite (18) and, as a consequence, the activation energy of oxidation. Thus, it seems important to take into account the diversity of a suspension of pyrite particles to establish a relationship between the electrochemical behavior and the chemical or physical transformation that occurs during the different steps of their oxidation by *T. ferrooxidans*.

The aim of this article is to describe more precisely the mechanisms of the bacterial oxidation of pyrite in relation to the content of the solution, bacterial growth, crystal corrosion, and measured redox potentials. For this purpose, experiments were performed in a pulp reactor equipped with a three-electrode open circuit, including an original pyrite-packed electrode (21) used to take into account the cathodic and anodic reactions occurring at or near the pyrite surface.

MATERIALS AND METHODS

Experimental device. Studies of the relationship between the electrochemical behavior of pyrite and the different steps of its chemical and physical evolution during bacterial oxidation were performed by using a reactor equipped with a platinum electrode and a special pyrite electrode.

Reactor. The reactor consisted of a Wheaton Pyrex-jacketed device, in which the temperature was maintained at 30°C by circulating water (Fig. 1). The vessel was open to the atmosphere. A special, original Teflon turbine was used to stir and oxygenate the medium efficiently.

Electrodes. The open-circuit potentials of the platinum electrode and pyrite bed electrode were measured versus a saturated calomel electrode (Fig. 1).

The platinum electrode (Ingold) had a special design to accept an external reference.

The pyrite electrode (Fig. 1) was made of a polyamide woven bag (pore size, 20 μm) which contained 1 g of pyrite grains (ca. 10^6 grains of the 53- to 80-μm fraction) packed around a platinum wire (Tacussel Pt1). The bag was closed by heat sealing.

The reference electrode was a saturated calomel electrode (SCE Ingold reference), which was placed into a water-jacketed compartment, connected to the platinum electrode by a plastic tube (Fig. 1). The filling solution for the reference electrode compartment and the connector was a

* Corresponding author.

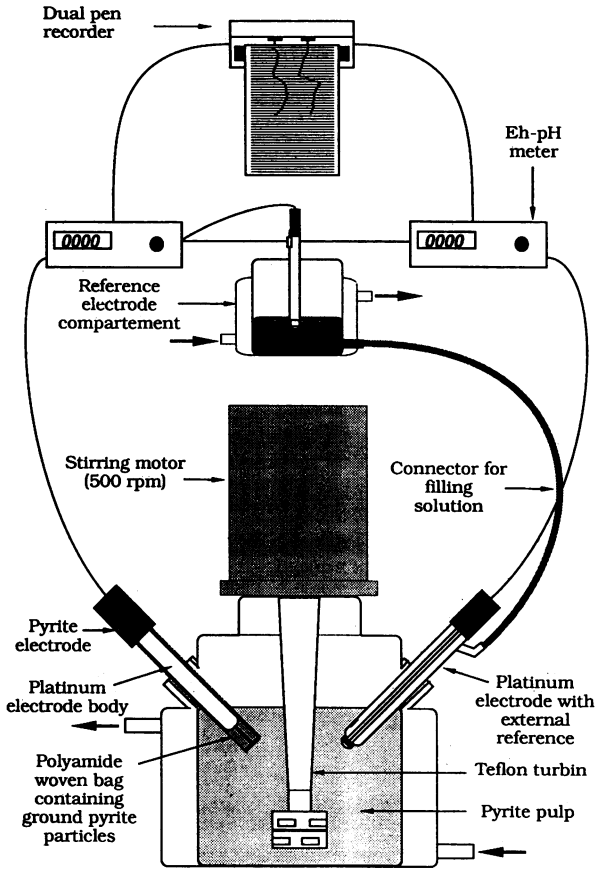

FIG. 1. Diagram of the three-electrode open circuit. The leaching reactor is equipped with a platinum electrode and a special pyrite electrode (packed ground-pyrite electrode).

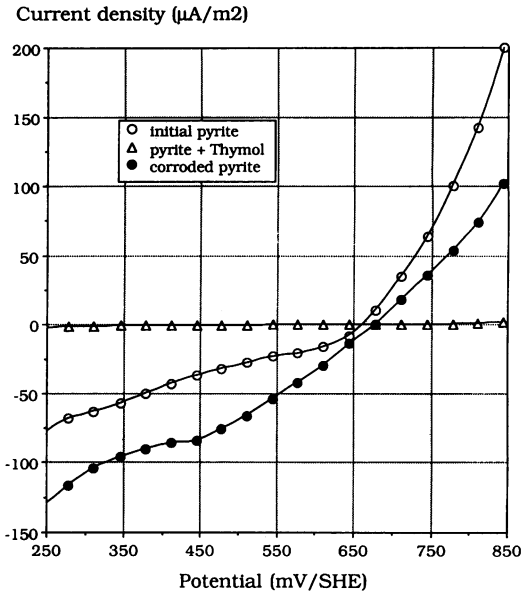

FIG. 2. Intensity-potential curves of packed ground-pyrite electrode in the nutrient medium.

K_2SO_4 (25 g liter^{-1}) solution. The potential of this electrode, relative to the standard hydrogen electrode at 30°C, was 242 mV.

Electronics. Both pyrite and platinum electrode potentials were simultaneously measured by two E_h-pH meters (Tacussel PHN 78 and MVIT-NUM) and recorded on a dual-pen recorder (Phillips PM 8222) (Fig. 1). The potentials reported here were recalculated to standard hydrogen electrode (SHE) as a reference.

Sulfide. The pyrite, originating from a sedimentary deposit in Spain (Logroño), had minor impurities (total, 0.4%) and should be considered from geological point of view as a natural pure pyrite. After dry grinding and wet sifting, the fraction (53 to 80 µm) was selected and analyzed; Fe and S contents were 46.23 and 52.97% (wt/wt), respectively. Chemical and electron microprobe analysis (SX Cameca) revealed traces of arsenic (0.3%) and of Ti and Ni (0.1%). The voltametric studies (intensity-potential curves) of the electrochemical properties of the initial pyrite revealed a rest potential around 660 mV per SHE in the nutrient medium (Fig. 2). The specific surface area (1.11 m^2 g^{-1}) was determined by a gas adsorption method using krypton as the adsorbate. Diffuse reflectance spectra of the mineral surface were recorded on a Fourier Transform Infrared Spectrophotometer (Bruker IFS 88) equipped with a mercury-cadmium-telluride detector in association with a diffuse reflectance attachment (Harrick Corp.). This device allowed the investigation of mineral surfaces and the organic species adsorbed on them (9, 25).

Bacteria and nutrient medium. The chemolithotrophic, gram-negative acidophilic bacterium *T. ferrooxidans* was provided by the Deutsche Sammlung von Mikroorganismen (DSM 583). The nutrient medium, used throughout this study, contained the following (per liter of distilled water): KH_2PO_4, 0.4 g; $MgSO_4 \cdot 7H_2O$, 0.4 g; and $(NH_4)_2SO_4$, 0.4 g. The pH was adjusted to 1.8 with 30 ml of H_2SO_4 (1 N) and the nutrient medium was sterilized at 120°C for 20 min. The medium was acidified to allow good bacterial growth without precipitation of iron oxyhydroxide species which occurs at a pH greater than 2.0. After being separately autoclaved in water (two times), sterilized pyrite was added to the medium to obtain a 2% weight pulp. The infrared spectra showed that the pyrite surface was not modified by autoclaving. The reactor was then inoculated with an actively growing culture to produce an initial population of 10^7 bacteria ml^{-1}. Bacterial growth measurements were made by direct microscopic counting at ×400 magnification with a Thoma cell (0.01-mm depth).

An inoculated reactor with thymol (2-isopropyl, 5-methyl, phenol $C_{10}H_{14}O$) served as the control. The bacteriostatic properties of thymol are known, and its effect on the electrochemical properties of pyrite will be discussed later in this article.

Solution analysis. The iron(II) concentration was determined by a standard 2,2′-bipyridyl colorimetric method (Merck Reagents). The total iron and sulfur analyses were made by using inductive coupled plasma analysis (ICP Jobin Yvon JY 32) using an internal Sr-HCl standard (0.6% of matrix) which improved the precision of the measurements. Sampling in the reactor did not exceed 0.25% of the total volume, and the evaporation rate was taken into account for the calculation of the concentration.

Microscopy observations. Scanning electron microscopy (SEM) observations were carried out on a conventional F.B. Cambridge Stereoscan Microscope equipped with a Si-Li Princeton detector. Samples were collected in the reactor

and dried under an O_2-free atmosphere to preserve the surface and the corrosion pits. Optical microscopy observations were made with a Nachet microscope (NS 400), equipped with a Nomarsky interferential contrast device. The high optical resolution permitted the simultaneous observation of the bacteria and corroded pyrite grains.

Comparison of the iron and sulfur oxidation rates. A derivative ratio of the oxidation rates of sulfur and iron was used to compare these data more accurately. This ratio (R_{ox}) is written in the following form: $R_{ox}(t) = d(SO_4)/dt \times [d(Fe)/dt]^{-1}$, where ($SO_4$) and (Fe) represent the amounts in moles per liter of sulfate and iron solubilized in the solution, respectively. It can be used to show the incongruent dissolution of pyrite. The R_{ox} value for a congruent dissolution of a pure pyrite must be constant versus time and equal to 2. The R_{ox} ratio was obtained after a polynomial regression (order 3) of experimental data. The polynomial equations of the regression curves corresponding to the iron and sulfate concentrations (in moles per liter), up to 30 days, were determined as follows:

$$(Fe) = 2.80 \times 10^{-4} - 1.30 \times 10^{-4}t + 1.81 \times 10^{-5}t^2 + 1.13 \times 10^{-6}t^3 \quad (r^2 = 0.999)$$

$$(SO_4) = 1.94 \times 10^{-2} - 6.09 \times 10^{-4}t + 8.76 \times 10^{-5}t^2 + 7.97 \times 10^{-7}t^3 \quad (r^2 = 0.995)$$

where t is the elapsed time and r is the regression coefficient.

The zero-order terms in each equation were in a good agreement with the initial concentrations of iron and sulfur species in the solution after pyrite addition and inoculation. After 30 days, the appearance of precipitates disturbed the calculation.

RESULTS

The changes in the redox potentials of the platinum and pyrite electrodes, the dissolution of iron and sulfur, and the SEM observation of corrosion patterns allowed the description of four main steps found during a bioleaching cycle.

Step I. The lag phase. Initially, ferric ions introduced with the inoculum were reduced (Fig. 3). The open-circuit potential of the platinum electrode converged around the pyrite potential (Fig. 4a). The open-circuit potential of pyrite decreased slightly and had a lower value than the previously defined rest potential in nutrient medium (Fig. 2). At the end of this lag phase (5 days in the present experimental conditions), platinum and pyrite electrodes had the same potential (640 mV per SHE). Iron and sulfur solubilizations were very weak (Fig. 5); therefore, the calculation of the R_{ox} ratio was not performed (Fig. 6).

The number of bacteria present in the liquid medium decreased (Fig. 7). Adsorption onto pyrite, which involved 90% of inoculated bacteria, began immediately after the inoculation, and the pH increased slightly (Fig. 7). No corrosion was observed by SEM examination (Fig. 8a). In the control treatment (with addition of thymol), except for iron(III) reduction (Fig. 3), no detectable evolution was noted.

Step II. The start of the dissolution. At the beginning of the second step, the ferrous ions produced in step I were quickly and completely oxidized (Fig. 3). After a small decrease of pyrite potential (1 day), both platinum and pyrite potentials increased simultaneously and exceeded the rest potential of pyrite (Fig. 4a). The pyrite potential, which was slightly higher than that of platinum during this increasing step, reached a stable value, about 80 mV lower than the platinum electrode potential.

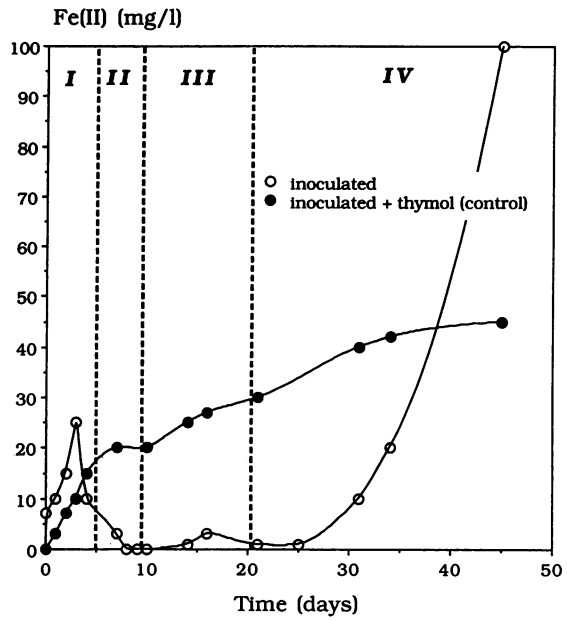

FIG. 3. Ferrous iron contents in solution versus time during the four steps (I, II, III, IV) of bioleaching.

The bioleaching process began, and the solubilization of iron and sulfur became significant (Fig. 5). The R_{ox} value of 2.5 indicated a preferential solubilization of sulfur (Fig. 6). The number of bacteria in the nutrient medium increased with the beginning of the exponential growth phase, and the pH began to decrease (Fig. 7). Corrosion patterns, as in the previous step, were not detectable by SEM even at high magnification (×6,000) (Fig. 8b).

In the control treatment, during this step and the following ones, only very little ferrous iron solubilization resulted from the chemical solubilization of pyrite in the nutrient medium (Fig. 3). The potentials remained low (Fig. 4c) and had a tendency to decrease slowly. The acidity was not greatly modified (results not reported), but the number of bacteria decreased (Fig. 7).

Step III. The superficial attack. The third step was dominated by the high content of ferric ions in solution (Fig. 5). The iron(II) concentration was very low (Fig. 3). An equilibrium between both potentials was reached around 80 mV (Fig. 4b).

Iron and sulfur solubilizations increased strongly (Fig. 5). The R_{ox} ratio indicated that sulfur was always preferentially solubilized over iron (Fig. 6); however, the R_{ox} ratio decreased and became stoichiometric after 18 days (R_{ox} = 2.01).

The increase in bacterial population in the nutrient medium corresponded to the last part of its exponential growth phase. The pH decreased constantly (Fig. 7). The first patterns of corrosion (Fig. 8c) were evident from the appearance of some cracks (0.6 μm wide).

In the control experiment, only a very small amount of ferrous iron was observed. In this treatment, both potentials showed similar decreases (Fig. 4c). The bacteria were not detectable by the direct counting method.

Step IV. The deep attack. Progressively after 25 days, ferrous ions appeared again but always in a very low concentration in comparison to the ferric ions (Fig. 3). The pyrite potential increased, and the platinum potential de-

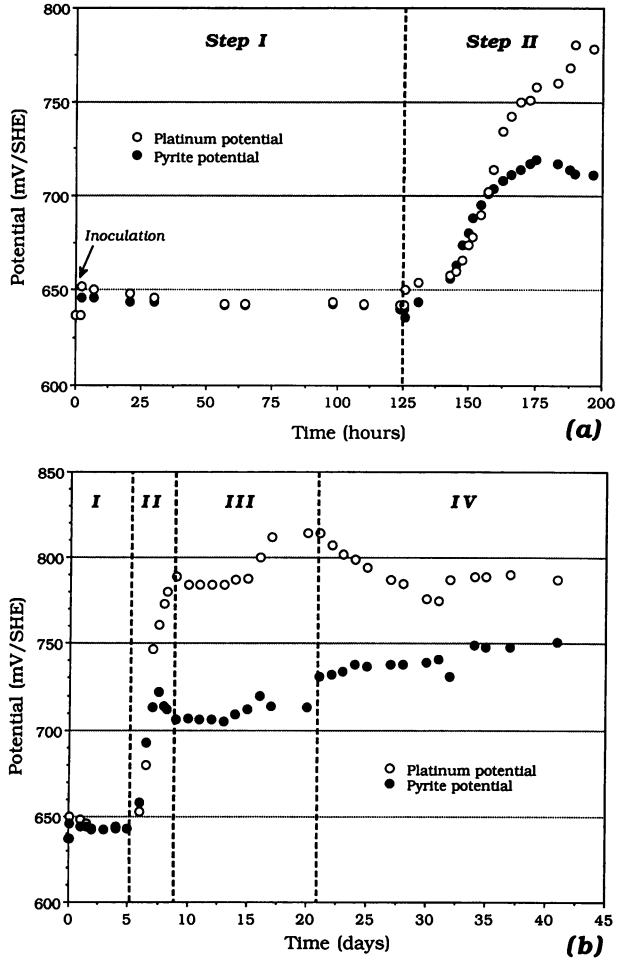

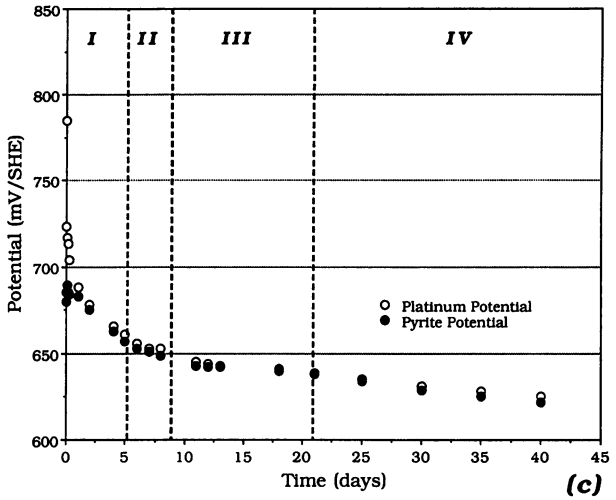

FIG. 4. Evolution of both pyrite and platinum potentials. (a) Details of the first two steps; (b) record of the four steps; (c) potentials in the control reactor without bacterial activity in the presence of thymol.

creased. After 30 to 40 days of bioleaching, the differences between the platinum and pyrite potentials were no more than 40 mV (Fig. 4b).

Iron and sulfur were always strongly solubilized as ferric sulfate. The preferential iron dissolution was supported by the low R_{ox} value of less than 2 (Fig. 6).

The bacterial population reached the stationary phase at the beginning of this step. The pH decreased strongly, reaching 1.3 after 45 days.

The SEM photographs showed hexagonal or square etched pits (internal diameter, about 2 μm) which penetrated the mineral to varying depths (Fig. 8d). The shape and the direction of the corrosion patterns seemed to be related to the cubic lattice of pyrite (16).

At the end of the experiment, it was observed that corrosion patterns were the same for the mineral grains sampled in pulp and those in the electrode bag.

The bioleaching experiment was repeated three times, and very similar relationships between the measured parameters were observed. Only a small delay in the lag phase (less than 1 day) and a small variation in the amount of solubilized species (less than 10%) were observed. By using a pure, carefully ground pyrite, a pure strain, and a 400-ml reactor, the reproducibility of the experimental results was improved. The previously described delineation of the bioleaching cycle was always observed.

DISCUSSION

The experimental setup allowed us to measure simultaneously the redox potential of a pyrite electrode and a platinum electrode over the entire bioleaching cycle, which revealed more accurately the different steps of the biooxidation process in relation to the evolution of pyrite solution and mineral parameters.

In this work, the properties of the population of *T. ferrooxidans* could be modified during leaching despite inoculation of a pure strain and may have influenced the redox potential of the solution and that of the mineral. Nevertheless, it appears, in particular with voltametric studies, that electrochemical properties of pyrite are modified by bacterial oxidation. In addition, this modification can certainly be

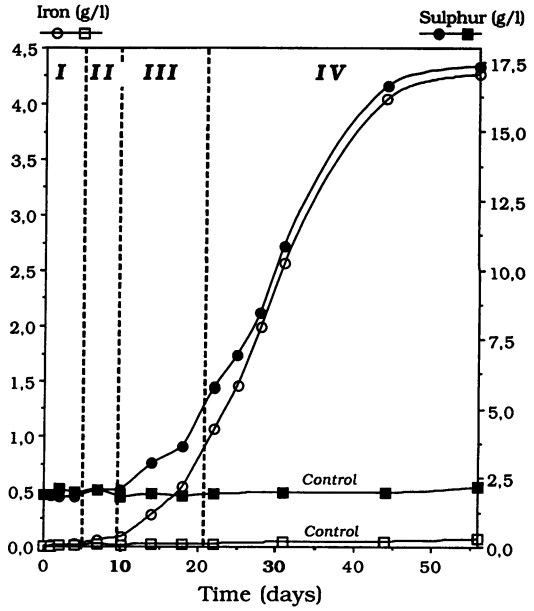

FIG. 5. Iron and sulfur contents in the leachate.

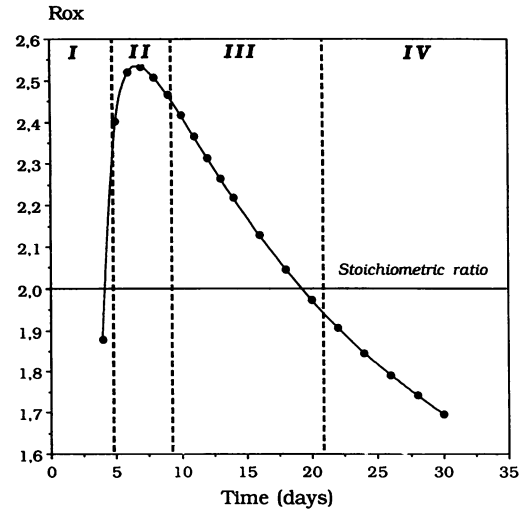

FIG. 6. Comparison of sulfur and iron oxidation rates (R_{ox} ratio versus time).

related to the presence of compounds on the pyrite surface which disturb the electrochemical behavior of pyrite, bacterial activity, and congruent dissolution of pyrite. Preliminary results (8) have shown that the surface layer can be strongly modified during bacterial leaching.

The packed-ground-pyrite electrode that contains 10^6 pyrite grains represents the great diversity of pyrite grains and, in particular, the different crystalline orientations and surface properties. This type of electrode shows a higher sensitivity towards the phenomena which occur at the mineral interface. By the formation inside the electrode of a microenvironment accessible to the bacteria, diverse bacterial and chemical reactions at the interface can take place and be more extensively integrated. The pyrite potential is also related to the presence of superficial pellicular phases

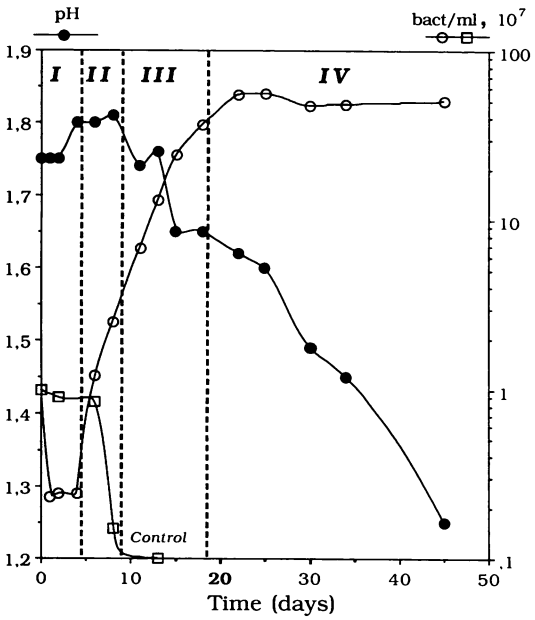

FIG. 7. Evolution of pH and bacterial growth.

(8) that are better randomly distributed in a ground-pyrite electrode than in a polished-pyrite electrode.

The platinum and pyrite electrode potentials are related to each other and to the parameters measured in solution (pH, bacterial growth, and sulfate and ferric ions in solution, etc.). The difference between both potentials corresponds to different electrochemical behaviors of the electrodes. While the platinum electrode is inert and reflects the redox potential of the pulp suspension, the pyrite electrode can react with ferric ions, dissolved oxygen, protons (acid), and bacteria present in the solution and the measured potential is a typical mixed potential. As mentioned earlier (24), the overall process of the dissolution of a pyrite is the sum of cathodic and anodic reactions occurring at the pyrite surface. The anodic process is a complex collection of oxidation reactions in which the pyrite reacts mainly with water to produce ferric ions, sulfates, and protons (equation 1) or ferrous ions and elementary sulfur (equation 2) when the acid strength increases (1):

$$FeS_2 + 8H_2O \rightarrow Fe^{3+} + 2SO_4^{2-} + 16H^+ + 15e^- \quad (1)$$

$$FeS_2 \rightarrow Fe^{2+} + 2S^0 + 2e^- \quad (2)$$

This second reaction shows a possible pathway for the formation of a sulfur-passive film.

The anodic process has been discussed (18) in terms of a two-layer system, where one layer is associated with the oxidation of iron(II) to iron(III) and the other involves the oxidation of sulfide (S_2^{2-}). The sulfide is oxidized through intermediates such as thiosulfate, elemental sulfur, or sulfate. The electrons are transferred to a cathodic site (at the mineral surface or on the bacteria) where the principal reaction is an oxygen reduction process:

$$O_2 + 4H^+ + 4e^- \rightarrow 2H_2O \quad (3)$$

Concurrently the ferric ion may be reduced to ferrous ion on the pyrite surface. Assuming that this process is controlled by the Fe(II)-Fe(III) couple, the stoichiometric equation has been postulated (12):

$$FeS_2 + 8H_2O + 14Fe^{3+} \rightarrow 15Fe^{2+} + 2SO_4^{2-} + 16H^+ \quad (4)$$

The presence of an active *T. ferrooxidans* culture provokes and catalyzes the completion of a cyclic process by regenerating the ferric ions through the oxidation of ferrous ions.

The bacterial growth and oxidation of sulfide are inhibited in the control treatment by the presence of thymol. The bacteriostatic effect of thymol is well understood; however, thymol can also modify the electrochemical behavior of mineral particles. Figure 2 exhibits the electrochemical inhibition effect of this molecule: a pyrite treated with thymol is not electrochemically active. The diffuse reflectance spectra (Fig. 9) confirm the presence of an adsorbed species on a mineral surface. The infrared spectrum showed in Fig. 9, spectrum a, indicates the methyl-stretching vibrations of the adsorbed thymol molecule that can be, in a first approximation, decomposed as follows: asymmetric 2,961 and symmetric 2,871 cm^{-1} stretching vibration of the two methyl groups of the isopropyl radical; 2,927 and 2,871 cm^{-1} in phase symmetric CH_3 stretch of the methyl group in α of the hydroxyl function in Fermi resonance with a CH_3 deformation overtone. The surface coverage can be sufficient to saturate all of the reactive sites of pyrite grains and, thus, to inhibit bacterial nutrition.

Finally, the study of chemical, electrochemical, and bacterial processes involved in pyrite bioleaching has proven that the redox potential is controlled by the ferrous-ferric

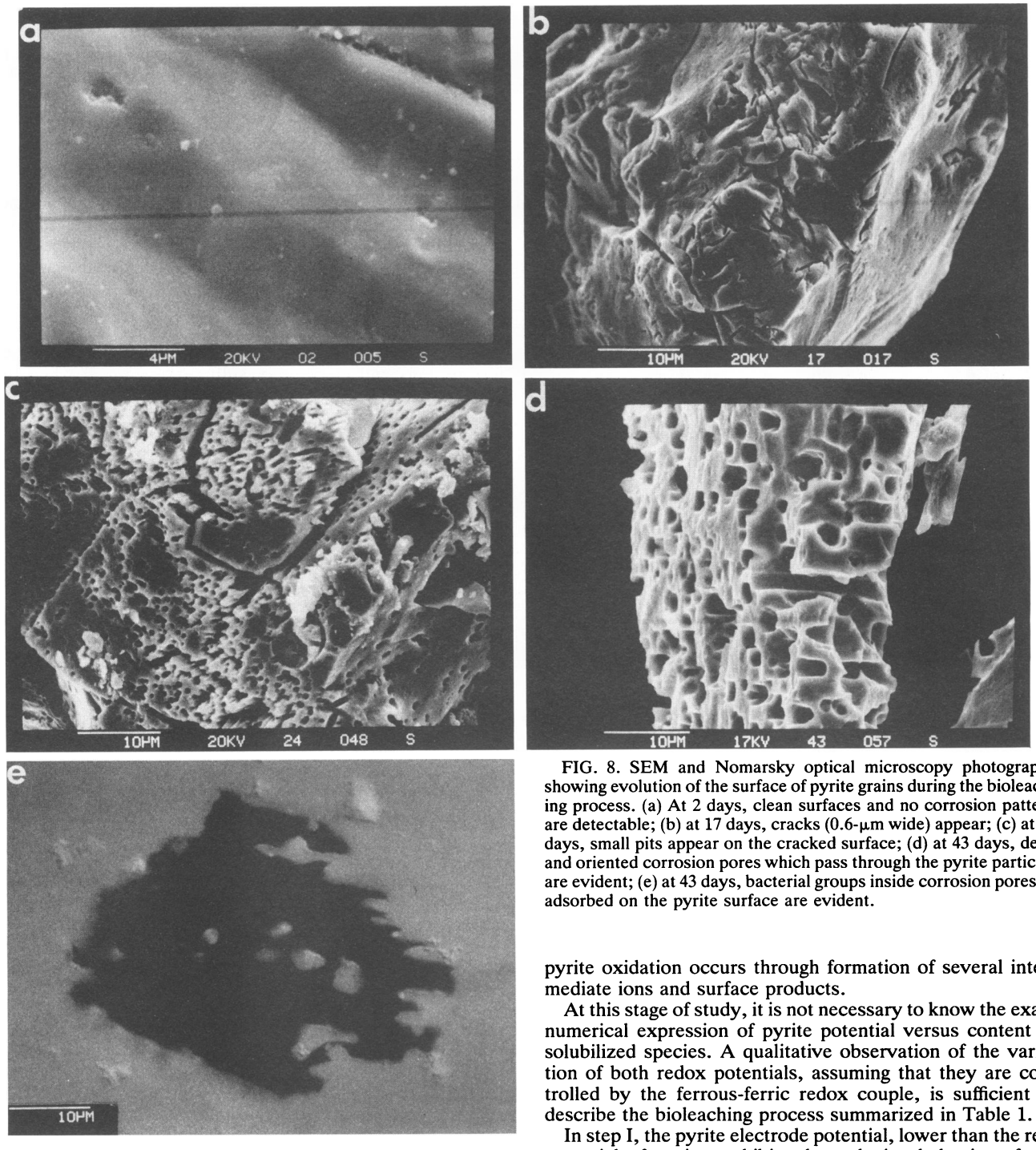

FIG. 8. SEM and Nomarsky optical microscopy photographs showing evolution of the surface of pyrite grains during the bioleaching process. (a) At 2 days, clean surfaces and no corrosion pattern are detectable; (b) at 17 days, cracks (0.6-µm wide) appear; (c) at 24 days, small pits appear on the cracked surface; (d) at 43 days, deep and oriented corrosion pores which pass through the pyrite particles are evident; (e) at 43 days, bacterial groups inside corrosion pores or adsorbed on the pyrite surface are evident.

redox couple (10, 20). Pyrite and platinum redox potentials are expressed by the following Nernst's equation: $E = E_0 + (RT/nF) \times [\ln (Fe^{3+}/Fe^{2+})]$, where the standard potential E_0 and the (RT/nF) value are well defined under standard conditions for a platinum electrode. In the case of a pyrite electrode (22), differences were observed between the theoretical and the measured potentials, which can be explained by the existence of mixed potential, the influence of semiconducting properties, or the appearance and dissolution of some superficial species that were previously neglected (8); pyrite oxidation occurs through formation of several intermediate ions and surface products.

At this stage of study, it is not necessary to know the exact numerical expression of pyrite potential versus content of solubilized species. A qualitative observation of the variation of both redox potentials, assuming that they are controlled by the ferrous-ferric redox couple, is sufficient to describe the bioleaching process summarized in Table 1.

In step I, the pyrite electrode potential, lower than the rest potential of pyrite, exhibits the reducing behavior of the sulfide. The convergence and the stability of both potentials prove that a the balance of ferrous and ferric species exists at the mineral-solution interface. On the pyrite surface, ferric ions and molecular oxygen are reduced. The anodic reaction may involve the sulfur species.

In the second step, both potentials increase rapidly by bacterial oxidation of soluble ferrous iron which is mainly responsible for the potential wave. During a short time period of bioleaching, the pyrite potential, slightly greater than the platinum potential, shows that the mineral surface is the main oxidation area. The ferric ions produced are

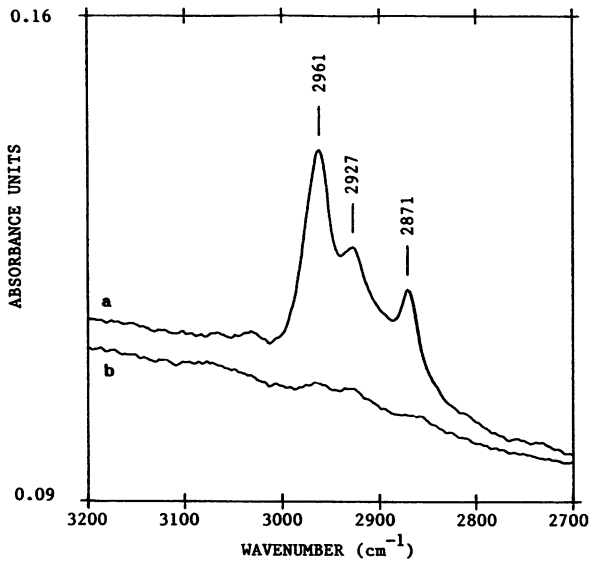

FIG. 9. Diffuse reflectance infrared spectra of pyrite treated with thymol (adsorbed on the surface) (a) and pyrite inoculated with bacteria (b).

diffused through the solution and are involved in the increase of redox solution potential. This step corresponds to a preferential oxidative solubilization of sulfur (Fig. 6) and increases in acidity and bacterial population (Fig. 7). It should be noted that the potential of pyrite becomes greater than the redox potential of the rusticyanine (680 mV per SHE) (14), which is considered to be the first electron acceptor of the *T. ferrooxidans* respiratory chain during iron oxidation. Yet, the pyrite becomes an electron donor and its bacterial oxidation is made easier. The nature of superficial species (like ferrous sulfate) produced during the bacterial oxidation of pyrite (8) could explain the incongruent oxidation of the pyrite (Fig. 6) and a certain degree of independence of iron and sulfur oxidations. Iron binding by the bacteria is too low to interfere with the measurement of iron content in the medium.

In the third step, the ferric ions present in a significant amount in solution can electrochemically oxidize the mineral (equation 4). The pyrite is attacked and its redox potential (Fig. 4) is lower than the platinum potential, which proves that the reductive behavior of the sulfide surface depends upon the interfacial iron(II)-iron(III) balance. Because of this aspect, the concentration of ferrous iron can be considered to be more important near the surface particles than in the solution where the iron oxidation rate increases. Thus, the difference between both potentials can be an indication of the intensity of the attack of pyrite and the ability of bacteria to regenerate ferric ions through the oxidation of ferrous ions.

In the last step, a progressive decrease of the difference between potentials of the pyrite and platinum electrodes is observed. The decrease of the platinum potential results from the formation, in the solution, of a detectable quantity of ferrous ions, which are not completely reoxidized by bacteria (Fig. 3). On the other hand, the increase of the pyrite potential reveals the higher concentration of ferric ions close to the sulfide surface, which certainly results from a bacterial activity inside the corrosion pores (Fig. 8d). Optical microscopic observation (Fig. 8e) shows bacteria

TABLE 1. Synthetic description of the different steps of the bacterial leaching process

Step	Processes involved		Potentials tendency[a,b]	V_{ox}[b,c]	R_{ox} ratio[b]	pH[b]	Bacterial growth[b]	Corrosion patterns
	At the pyrite surface	In the solution						
I	$Fe^{3+} \rightarrow Fe^{2+}$; $S^{2-} \rightarrow SO_4^{2-}$	Fe(II) ≫ Fe(III)	Py (−) Pt (−)	(0)	Undefined	(≡)	(−)	Undetectable
II	$FeS_2 \rightarrow Fe^{2+} + SO_4^{2-} + H^+$	$Fe^{2+} \rightarrow Fe^{3+}$ (Bact.); Fe(II) ≪ Fe(III)	Py (+) Pt (+)	(+)	>2 (+)	(−)	(−)	Undetectable
III	$FeS_2 + Fe^{3+} \rightarrow Fe^{2+} + SO_4^{2-} + H^+$	$Fe^{2+} \rightarrow Fe^{3+}$ (Bact.); Fe(II) = 0	Py (=) Pt (=) Pt − Py = 80 mV	(++)	≥2 (−)	(−)	(++)	Cracks and small pits
IV	$FeS_2 + Fe^{3+} \rightarrow Fe^{2+} + SO_4^{2-} + H^+$; $FeS_2 \rightarrow Fe^{2+} + S^0$	$Fe^{2+} \rightarrow Fe^{3+}$ (Bact.); Fe(II) > 0	Py (+) Pt (−) Pt→Py	(++)	<2 (−)	(−−)	(≡)	Deeply penetrating pores

[a] Py, pyrite; Pt, platinum.
[b] Symbols: (0), nil; (−−), strong decrease; (−), decrease; (=), stationary or with no significant evolution; (+), increase; (++), strong increase.
[c] V_{ox}, oxidation rate.

inside the corrosion patterns attached on the pyrite surface. Considering the development of corrosion patterns, the oxidation area seems to be mainly localized at the bottom of corrosion tunnels. The nonconical shape of pores observed by SEM confirms that their cylindrical sides are not always chemically and bacterially reactive. Nonattacked surfaces of sulfide grains may be partly responsible for the appearance of ferrous ions, produced by another anodic reaction (equation 2), which is favored by the increase of acid strength. On the other hand, the strong acidity could also inhibit the bacterial activity but not the oxidation. Acidity certainly promotes surface attacks but does not seem to be directly involved in deep leaching.

The specific surface areas of pyrite before and after bioleaching were 1.1 $m^2\ g^{-1}$ and 1.6 $m^2\ g^{-1}$, respectively. Bacterial oxidation created marked porosity and new surfaces in pyrite grains, and, as shown by the intensity potential curve of the leached pyrite, the abilities to produce an anodic current and to be oxidized were reduced by half (Fig. 2).

Pyrite oxidation is generally recognized as a complex phenomenon that includes oxidation and reduction processes and solid-solution equilibria involving several intermediate reactions and products (ions and solids products). In addition, the rate of oxidation depends on the semiconducting properties of sulfides (4, 7). For the pyrite sample used in these studies, the presence of a very small amount of arsenic (0.3%) can generate an n-type semiconducting effect and create mineral defects, both of which can affect bacterial oxidation (4).

In conclusion, the use of a special pyrite-particle electrode makes it possible to distinguish the different steps of pyrite leaching and corrosion, or weathering by *T. ferrooxidans*, and also suggests the reactions involved in a ground-particle leaching device. (i) Step I and step II can be considered as evolution stages controlled by surperficial phenomena, where the oxidation of sulfide and sulfur is favored. (ii) Step III is controlled essentially by the ferric ions produced in the leachate which can oxidize the mineral. (iii) Finally, step IV is a stage controlled by the crystalline structure; oxidation areas are localized inside the deep corrosion pores.

The integration of the overall electrochemical processes that occur on the pyrite surface shows the close relationship between both redox potentials (pyrite and leach solution) and the bacterial activity.

ACKNOWLEDGMENTS

We are extremely grateful to A. Kholer (Université de Nancy I) and P. Villecourt (Centre de Pédologie Biologique Nancy) for their participation in the microscopy observations. We also gratefully acknowledge the contribution of G. Belgy (Centre de Pédologie Biologique Nancy) for chemical analysis. Thanks are expressed to S. Martin and to J. Mielczarsky.

REFERENCES

1. **Bailey, L. K., and E. Peters.** 1976. Decomposition of pyrite in acids by pressure leaching and anodization: the case for an electrochemical mechanism. Can. Met. Quart. **15:**333–344.
2. **Basaran, A. H., and O. H. Tuovinen.** 1987. Iron pyrite oxidation by *Thiobacillus ferrooxidans*: sulfur intermediates, soluble end products and changes in biomass. Coal Preparation **5:**39–55.
3. **Berthelin, J.** 1987. Des bactéries pour extraire des métaux. La Recherche **188:**720–725.
4. **Choi, W. K., and A. E. Torma.** 1989. Electrochemical and semiconducting aspects of pyritic coal desulfurization by *Thiobacillus ferrooxidans*, p. 1–10. *In* Third International conference on processing and utilization of high-sulfur coals, Ames, Iowa, 14–17 November 1989.
5. **Colmer, A. R., and M. E. Hinkle.** 1947. The role of microorganisms in acid mine drainage: a preliminary report. Science **106:**253–256.
6. **Colmer, A. R., K. Temple, and M. E. Hinkle.** 1949. An iron-oxidizing bacterium from the drainage of some bituminuous coal mines. J. Bacteriol. **59:**317–328.
7. **Crundwell, F. K.** 1988. The influence of the electronic structure of solids on the anodic dissolution and leaching of semiconducting sulfide minerals. Hydrometallurgy **21:**155–190.
8. **de Donato, P., C. Mustin, J. Berthelin, and P. Marion.** 1991. An infrared investigation of pellicular phases observed on pyrite by scanning electron microscopy during its bacterial oxidation. C. R. Acad. Sci. Paris Sér. II **312:**241–248.
9. **de Donato, P., J. M. Cases, M. Kongolo, L. Michot, and A. Burneau.** 1990. Infrared investigation of amylxanthate adsorption on galena: influence of oxidation, pH and grinding. Colloids Surf. **44:**207–228.
10. **Ehrlich, H. L.** 1990. Geomicrobiology, 2nd ed. Marcel Dekker, Inc. New York.
11. **Ehrlich, H. L., and C. L. Brierley.** 1990. Microbial mineral recovery. McGraw-Hill Publishing Co., New York.
12. **Garrels, R. M., and M. E. Thompson.** 1960. Oxidation of pyrite by iron sulfate solutions. Am. J. Sci. **258A:**57–67.
13. **Hutchins, S. R., M. S. Davidson, J. A. Brierley, and C. L. Brierley.** 1986. Microorganisms in reclamation of metals. Annu. Rev. Microbiol. **40:**311–336.
14. **Ingledew, W. J.** 1986. Ferrous iron oxidation by *Thiobacillus ferrooxidans*, p. 23–33. *In* H. L. Ehrlich and D. S. Holmes (ed.), Workshop on biotechnology for the mining, metal refining and fossil fuel processing industries. John Wiley & Sons, Inc., New York.
15. **Karamanev, D. G., and L. N. Nikolov.** 1986. Influence of some physicochemical parameters on bacterial activity of biofilm: ferrous iron oxidation by *Thiobacillus ferrooxidans*. Biotechnol. Bioeng. **31:**295–299.
16. **Keller, L., and L. F. Murr.** 1982. Acid-bacterial and ferric sulfate leaching of pyrite single crystals. Biotechnol. Bioeng. **24:**83–96.
17. **Lizama, H. M., and I. Suzuki.** 1989. Rate equations and kinetic parameters of the reactions involved in pyrite oxidation by *Thiobacillus ferrooxidans*. Appl. Environ. Microbiol. **55:**2918–2923.
18. **Lowson, R. T.** 1982. Aqueous oxidation of pyrite by molecular oxygen. Chem. Rev. **82:**461–497.
19. **McKibben, M. A., and H. L. Barnes.** 1986. Oxidation of pyrite in low temperature acidic solutions: rate laws and surface textures. Geochim. Cosmochim. Acta **50:**1509–1520.
20. **Moses, C. O., D. K. Nordstrom, J. S. Herman, and A. L. Mills.** 1987. Aqueous pyrite oxidation by dissolved oxygen and by ferric iron. Geochim. Cosmochim. Acta **51:**1561–1571.
21. **Mustin, C., P. Marion, J. Berthelin, P. de Donato, and M. Monroy.** 1991. An original technique to study bacterial oxidation of pyrite: packed electrodes. C.R. Acad. Sci. Paris Ser. II **312:**1197–1203.
22. **Pesic, B., D. J. Oliver, and P. Wichlacz.** 1988. An electrochemical method of measuring the oxidation rate of ferrous to ferric iron with oxygen in the presence of *Thiobacillus ferrooxidans*. Biotechnol. Bioeng. **33:**428–439.
23. **Silverman, M. P.** 1967. Mechanism of bacterial pyrite oxidation. J. Bacteriol. **94:**1046–1051.
24. **Singer, P. C., and W. Stumm.** 1970. Acidic mine drainage: the rate-determining step. Science **167:**1121–1123.
25. **Sivamohan, R., P. de Donato, and J. M. Cases.** 1990. Adsorption of Oleate species at the fluorite-aqueous solution interface. Langmuir **6:**637–644.
26. **Torma, A. F.** 1986. Biohydrometallurgy as an emerging technology, p. 23–33. *In* H. L. Ehrlich and D. S. Holmes (ed.), Workshop on biotechnology for the mining, metal refining and fossil fuel processing industries. John Wiley & Sons, Inc., New York.